Semiconductor Physics, Quantum Electronics & Optoelectronics, 2013. V. 16, N 4. P. 344-348.

PACS 42.50.Tx

Generation of optical vortices in rotating uniaxial crystal for light propagation along the perpendicular to its optical axis

B.V. Sokolenko, A.F. Rubass, A.V. Volyar
Taurida National University, Department of General Physics,
4, Vernadsky Ave., 95007 Simferopol, Ukraine,
Phone: +38(066)574-73-02, e-mail: simplexx.87@gmail.com

Abstract. We have experimentally considered evolution of the Gaussian beam propagating nearly perpendicular to the uniaxial crystal axis. Also we have analyzed the spin and orbital angular momenta and found oscillations of the angular momentum when the crystal optical axis is rotated.

Keywords: angular momentum, singular beam, polarization, optical vortex, umbilics.

Manuscript received 10.07.13; revised version received 03.09.13; accepted for publication 23.10.13; published online 16.12.13.

1. Introduction

It is well known that the Gaussian beam propagates perpendicular to the crystal optical axis and splits into the ordinary and extraordinary ones. The ordinary beam transmits through the crystal as through the isotropic medium while the extraordinary beam is elliptically deformed [1]. In case the beam bears the optical vortex then the crystal changes the singular structure of the vortex. The slight changes of the crystal parameters can result in the critical transformations of the phase singularity [2-4]. However the question of the vortex generation in this case remains open.

Thus the aim of the presented paper is the experimental study of the birth and death of phase singularities processes when the beam propagates nearly perpendicular the crystal optical axis.

2. The basic representations

Let us consider the total representations of the properties of the monochromatic optical fields following the paper [5].

In the paraxial approximation, the electromagnetic field can be written in the form:

$$E = E_x + E_y,\ \mathrm{H} = H_x + H_y \tag{1}$$

or

$$\begin{Bmatrix} E_j \\ H_j \end{Bmatrix} = \exp(ikz) \times \left(\begin{Bmatrix} e_x \\ e_y \end{Bmatrix} u_j + \frac{i}{k} e_z \begin{bmatrix} \partial/\partial x \\ \partial/\partial y \end{bmatrix} u_j \right), \tag{2}$$

where $j = x, y$ and k stand for the wavenumber.

The complex amplitude takes the form

$$u_j = A_j(r, z) \exp[ik\varphi_j(r, z)] \tag{3}$$

Then the Poynting vector is

$$S = \frac{c}{2\pi} \mathrm{Re}\Big(\big[E_X \times H_r^*\big] + \big[E_r \times H_X^*\big] + \big[E_X \times H_X^*\big] + \big[E_Y \times H_Y^*\big] \Big). \tag{4}$$

After substitution of Eq. (3) into Eq. (4), we can select the energy flux associated with the spin-orbital momentum [5]

$$S_c = -\frac{ic}{16\pi k} \Big[e_z \times \nabla (u_X u_Y^* - u_X^* u_Y) \Big], \tag{5}$$

while the spin angular momentum (SAM) is

$$L_c = \frac{1}{c^2}\int [r \times S_c]\, d^2 r\,. \qquad (6)$$

At the same time, the volume density of the SAM is written as $\frac{i}{8\pi\omega}\left(u_X u_Y^* - u_X^* u_Y\right)$. Thereof, the local SAM can be expressed by means of the Stokes parameters:

$$A_c = \frac{i\,(u_X u_Y^* - u_X^* u_Y)}{|u_X|^2 |u_Y|^2} = \frac{S_3}{S_0}\,, \qquad (7)$$

where

$$S_0 = |\nabla_{\perp E}|^2 \text{ and } S_3 = i(\partial_X E^* \partial_Y E - \partial_X E \partial_Y E^*)\,.$$

The local SAM equal to the ratio S_3/S_0 cannot exceed "1". In the case of the circular polarized beam, we have $A_c = \pm 1$ or $\pm\hbar$ per photon.

The second part in Eq. (4) presents the orbital angular momentum (OAM) written in the form

$$\boldsymbol{S}_o = e_z \boldsymbol{S}_\square + \boldsymbol{S}_{\perp X} + \boldsymbol{S}_{\perp Y} \qquad (8)$$

with $e_z \boldsymbol{S}_\square$ being the longitudinal flux, while the sum $S_{\perp X} + S_{\perp Y}$ is the transverse flux:

$$\boldsymbol{S}_\square = \frac{c}{8\pi}(A_X^2 + A_Y^2),\ \boldsymbol{S}_{\perp j} = \frac{ic}{16\pi k}(u_j \nabla u_j^* - u_j^* \nabla u_j)\,. \qquad (9)$$

Thus, the total OAM of the beam is

$$L_o = \frac{1}{c^2}\int [r \times (S_{\perp X} + S_{\perp Y})]\, d^2\,. \qquad (10)$$

OAM is associated with the spatial beam structure. In contrast to the SAM, the OAM depends on the coordinate transformations.

Thus, the angular momentum can contain some parts related to different degrees of freedom of the light wave: SAM is charged with the polarization state, whereas OAM characterizes the beam as a whole, its geometry and space movement [5].

In the case of the anisotropic medium, the changes in the ordinary and extraordinary beams are also related with SAM. However, different parts of the beam undergo different transformations. The beam is spatially depolarized. SAM decreases. At the same time, the polarized beam components are transformed, too. These processes partially compensate each other. (When the beam propagates along the crystal optical axis the transformations of SAM compensate each other precisely.)

3. Experimental study of the spin-orbital coupling

It is known that conversion of the elliptical singular beams has periodical features taking place along the beam axis z propagating along the perpendicular to the crystal optical axis [2]. The most interesting case springs up when the beam propagates nearly perpendicular to the optical axis with the deviation angle $\alpha \sim 7°$ so that $\sin\alpha_0 \approx \alpha_0$. Besides, the transformation dynamic of the beam cross-section is very complex process, because the ordinary and extraordinary beams lay partially upon each other for the small deviation angle α_0. As the result, we obtain the complex polarization pattern containing the chain of the polarization singularities from the lemon, star and monster [7].

The experimental set-up for studying the Gaussian beam evolution is shown in Fig. 1.

The Gaussian beam radiated from the He-Ne laser with the wavelength $\lambda = 0.6328$ μm splits with the plate Bs_1 forming together with the plate Bs_2 an interferometer. After transmitting the $\lambda/4$ plate, the beam gets the circular polarization in one interferometer arm. Then, the beam is focused by the lens L_1 at the input crystal Cr face with beam waist $w_0 \approx 0.02$ mm. The crystal (SiO_2) is mounted in the specially designed optical stand and turned at the angle α_0 relatively to the beam axis. Besides, the crystal optical axis can turn at the angle ψ. Then, the beam is collimated by the lens L_2, passes through the circular polarizer $\lambda/4 - P$ being recorded by the CCD camera after mixing with the reference beam.

In order to understand the obtained results, let us consider beam propagation nearly perpendicular to the uniaxial crystal optical axis following the paper [1]. The

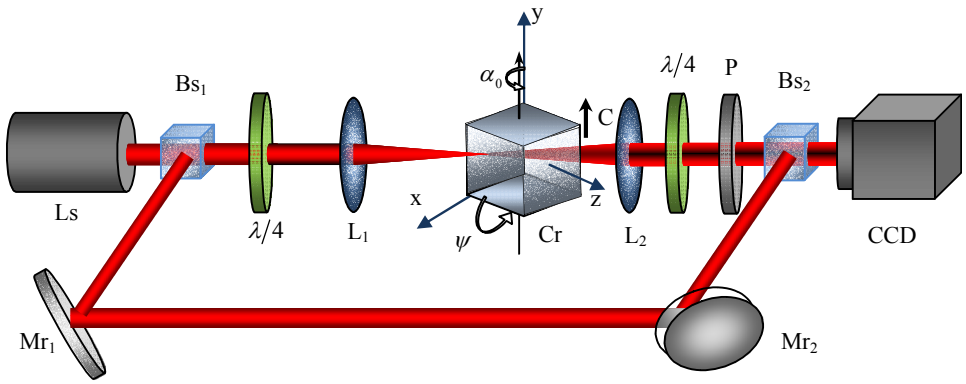

Fig. 1. The schematic representation of experimental set-up.

complex amplitudes of the ordinary $\widetilde{E}_x$ and extraordinary $\widetilde{E}_y$ components, in the coordinates related with the crystallographic axes, have the form

$$\widetilde{E}_x = \exp\left[-\left(X_o^2 + Y_o^2\right)/ w_o^2\sigma_o - f_o\right] / \sigma_o , \qquad (11)$$

$$\widetilde{E}_y = \frac{i}{\sqrt{\sigma_x\sigma_y}} \exp\left[-\frac{X_e^2}{w_e^2\sigma_x} - \frac{Y_e^2}{w_e^2\sigma_y} - f_e\right] , \qquad (12)$$

where: $z_o = k_1 w_o^2/2$, $z_x = k_2 w_e^2/2$, $z_y = k_2 w_e^2 n_1^2/2n_2^2$,

$\sigma_o = 1 - iz/z_o$, $\sigma_x = 1 - iz/z_x$, $\sigma_y = 1 - iz/z_y$,

$X_o = x + i\alpha_o z_o \cos\psi$, $Y_o = y + i\alpha_o z_o \sin\psi$, $X_e = x + i\alpha_x z_x \cos\psi$,

$Y_e = y + i\alpha_y z_y \sin\psi$, $f_o = a_o^2 k_1 z_o/2$,

$f_e = a_x^2 k_2 z_x \cos^2\psi/2 + a_y^2 k_1 n_1/n_2 z_y \sin^2\psi/2$.

In the laboratory referent frame, coordinate transformation is as follows:

$$x = x_1\cos\psi + y_1\sin\psi , \quad y = -x_1\sin\psi + y_1\cos\psi \qquad (13)$$

while basic transformation has the form

$$E_x^1 = E_x\cos\psi - E_y\sin\psi , \quad E_y^1 = E_x\sin\psi + E_y\cos\psi . \qquad (14)$$

The theoretical and experimental patterns shown in Fig. 2 correspond to the intensity distributions for the right-hand polarized component.

Fig. 2 illustrates the intensity distribution in the nearly standard conoscopic pattern. A small asymmetry of the pattern is the result of a slight inclination ($\alpha \sim 2^\circ$) of the crystal and the beam axes. At the same time, the asymmetry type and shape of the beam cross-section can be controlled by the α_0 and ψ angles.

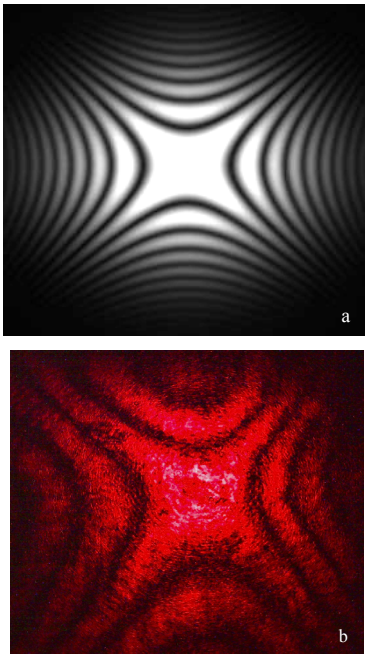

Fig. 2. The conoscopic patterns of the beam field after the crystal with $z = 2$ cm: theory (*a*) and experiment (*b*).

Evidently, the expression (7) enables us to calculate SAM provided that we can define the Stokes parameters S_3 and S_0 experimentally. These measurements permit to implement our experimental set-up. This process is demonstrated in Fig. 3. The shown curves are SAM as a function of the ψ angle, when the angle α_0 is a parameter. Rotation of the optical axis (the angle ψ comes to the oscillations of SAM. The angles α_0 are chosen in such a way that the ordinary and extraordinary beams do not split along the crystal length for account of the crystal birefringence. Within a rather large range of the α_0 angles, we observe large amplitude oscillations.

However, there are some angles where the oscillation amplitude of SAM is very small. In our opinion, this process is related with the conversion of the spin and orbital angular momenta. Indeed, for the relatively large angles α_0 the ordinary and extraordinary beams are partially separated. The shape of the beam cross-section is strongly distorted increasing OAM. In its turn, SAM decreases for account of the spin-orbital coupling (see the next Section). OAM can be experimentally estimated as a ratio of the average small and large ellipse axes. Such a process is illustrated in Fig. 4.

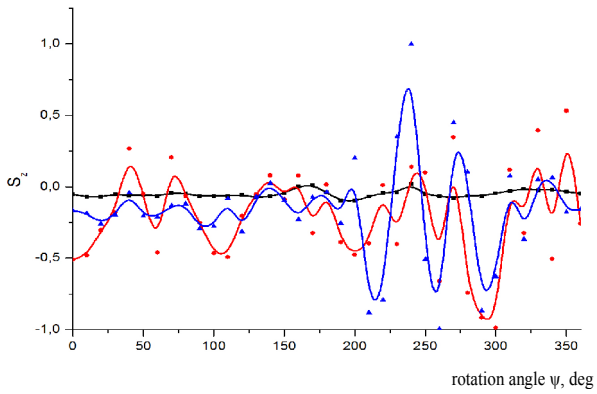

Fig. 3. The SAM dynamics plotted for $\alpha_0 = 7^\circ$ (red line ●), $\alpha_0 = 17^\circ$ (blue line ▲) and $\alpha_0 = 23^\circ$ (black line ■). Rotational angle $\psi = 0\ldots360^\circ$.

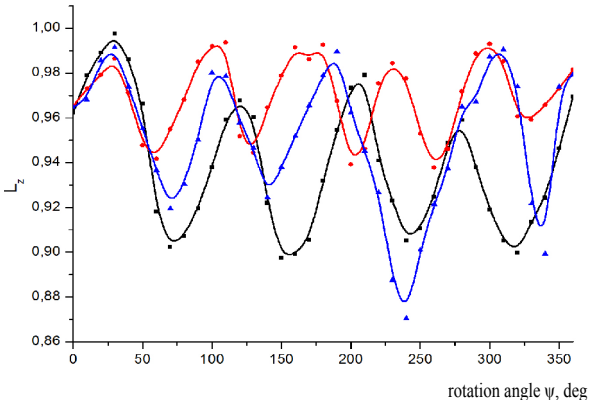

Fig. 4. The OAM dynamics plotted for $\alpha_0 = 7^\circ$ (red line ●), $\alpha_0 = 17^\circ$ (blue line ▲) and $\alpha_0 = 23^\circ$ (black line ■). Rotational angle $\psi = 0\ldots360^\circ$.

The comparison of the curves in Figs 3 and 4 shows that the growth of SAM is accompanied by decreasing the average OAM and vice versa.

4. Generation of the polarization singularities and the chains of optical vortices in the vector beam components

It is interesting to note that the strong downfall of the beam polarization ellipticity for some angles α_0 and ψ is related with not only the strong beam deformation but also the complex polarization distribution at the beam cross-section. But complex polarization distribution is always associated with the polarization singularities where the field in one of the circularly polarized components is equal to zero, i.e., the corresponding components carry over the optical vortices.

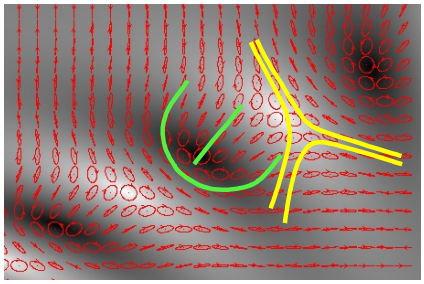

Fig. 5. The polarization distributions against the background of the right hand polarized component: $\alpha_0 = 2°$, $\psi = 210°$, $w_0 = 5$ μm, $z = 2$ cm.

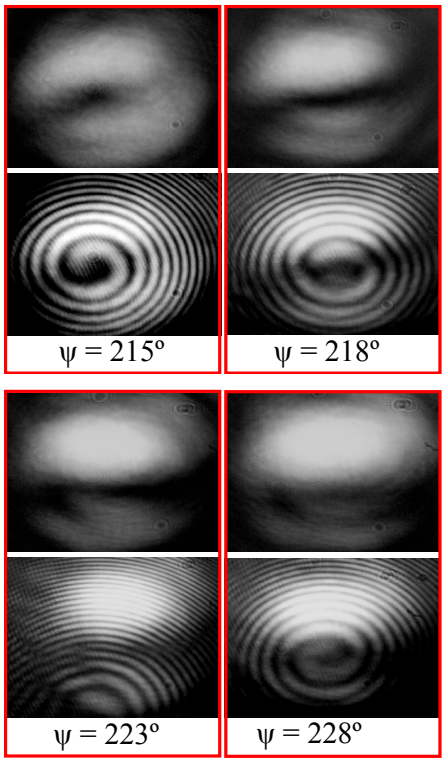

Fig. 6. The intensity distributions and interference patterns.

In order to estimate appearance of the polarization singularities and optical vortices, let us make use of Eqs (11) and (12) for the relatively small α_0 angles within the range $\psi = 210°…300°$.

The polarization pattern shown in Fig. 5 illustrates the chain of the polarization singularities in the form of the point with circular polarization enclosed by the standard polarization tracery corresponding to the singularities of the lemon (green lines) and star (yellow lines) types separated by the line with linear polarization (*L*-line). Circular polarizations are positioned at the places with the zero intensity corresponding to the optical vortices in the other circular polarized components.

We have experimentally verified this effect, as it is shown in Fig. 6. The interference patterns in the form of the complex spirals show definitely that the corresponding circularly polarized components carry over the single-charged optical vortices. The vortices are not motionless: during rotation of SiO_2 crystal around *z*-axis, the vortex becomes to move and changes its geometry. The intensity minimum spreads and, finely, is separated into two vortices with opposite signs. Both vortices move separately, while the first one annihilates with another singularity at the periphery, and the latter one, with the opposite sign, still remains in the beam. The whole process has periodic recurrence and repeats every 90 degrees of crystal rotation.

5. Conclusion

Beam propagation perpendicular to the crystal optical axis breaks the circular symmetry. Naturally, the vortex conversion in this case results in transforming the orbital angular momentum. But now, three processes take part in the phenomenon: spatial depolarization, related with SAM; ellipticity of beam cross-section caused by OAM; generation of polarization singularities and optical vortices. The spin and orbital angular momentum are supplemented by the response of the crystal medium. It is the sum of these three processes that must reduce to conservation of the total angular momentum.

Recently, it was revealed that the extraordinary paraxial beam, when the initial beam has a circular symmetry, is subjected to the complex elliptical deformation. Such a geometrical transformation is conditioned by different scales along the *x*- and *y*-axes for the extraordinary beams in the crystals. Naturally, deformation distorts polarization distribution at the beam cross-section and restricts application of the conservation law for the angular momentum [6].

References

1. T.A. Fadeyeva, A.F. Rubass, B.V. Sokolenko, A.V. Volyar, The precession of vortex-beams in a rotating uniaxial crystal // *J. Opt. A: Pure Appl. Opt*. **11**(9), p. 53-55 (2009).

2. T.A. Fadeyeva, C.N. Alexeyev, B.V. Sokolenko M.S. Kudryavtseva, A.V. Volyar, Non-canonical propagation of high-order elliptic vortex beams in a uniaxially anisotropic medium // *Ukrainian Journal of Physical Optics*, **12**, p. 62-82 (2011).
3. A. Ciattoni, G. Cincotti, and C. Palma, Angular momentum dynamics of a paraxial beam in a uniaxial crystal // *Phys. Rev*. *E*, **67**, 036618 (2003).
4. K.Y. Bliokh, E.A. Ostrovskaya, M.A. Alonso, O.G. Rodriguez-Herrera, D. Lara, C. Dainty, Spin-to-orbital angular momentum conversion in focusing, scattering, and imaging systems // *Opt. Exp.* **19**, 26132 (2011).
5. A.Y. Bekshaev, M.S. Soskin, M. Vasnetsov, *Paraxial Light Beams with Angular Momentum*. Nova Science Publishers, New York, 2008, p. 112.
6. B.V. Sokolenko, M.S. Kudryavtseva, A.V. Zinovyev, V.O. Konovalenko, A.F. Rubass, Optical vortex conversion in the elliptic vortex-beam propagating orthogonally to the crystal optical axis: The experiment // *Proc. SPIE*, **8338** (D-8), p. 83380D-83380 (2011).
7. J.F. Nye, *Natural Focusing and Fine Structure of Light: Caustics and Wave Dislocations*. London, Institute of Physics Pub. Science, 1999, p. 328.